INTERNATIONAL JOURNAL OF HYDROGEN ENERGY 47 (2022) 33988–33998

Available online at www.sciencedirect.com

ScienceDirect

journal homepage: www.elsevier.com/locate/he

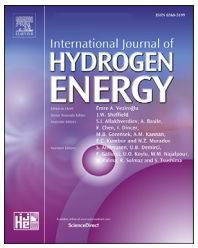

Physical insights into alkaline overall water splitting with NiO microflowers electrodes with ultra-low amount of Pt catalyst

Luca Bruno [a,b], *Sergio Battiato* [a,b], *Mario Scuderi* [c], *Francesco Priolo* [a], *Antonio Terrasi* [a,b], *Salvo Mirabella* [a,b,*]

[a] *Dipartimento di Fisica e Astronomia "Ettore Majorana", Università degli Studi di Catania, via S. Sofia 64, 95123, Catania, Italy*

[b] *IMM-CNR (Catania Università), via S. Sofia 64, 95123, Catania, Italy*

[c] *IMM-CNR, VIII strada 5, 95121, Catania, Italy*

HIGHLIGHTS

- Pt nanoparticles decoration of NiO microflowers.
- Effect of decoration on Hydrogen Evolution Reaction mechanism and on energy band modification of NiO.
- Overall water splitting with NiO and Pt–NiO electrodes in alkaline conditions.

ARTICLE INFO

Article history:
Received 20 June 2022
Received in revised form
27 July 2022
Accepted 1 August 2022
Available online 24 August 2022

Keywords:
Pt decorated NiO microflowers
Catalytic effect
Hydrogen evolution reaction
Overall water splitting
All NiO electrolyzer

ABSTRACT

Electrochemical water splitting represents a promising alternative to conventional carbon-based energy sources. The hydrogen evolution reaction (HER) is a key process, still if conducted in alkaline media, its kinetics is slow thus requiring high amount of Pt based catalysts. Extensive research has been focused on reducing Pt utilization by pursuing careful electrode investigation. Here, a low-cost chemical methodology is reported to obtain large amount of microflowers made of interconnected NiO nanowalls (20 nm thick) wisely decorated with ultralow amounts of Pt nanoparticles. These decorated microflowers, dispersed onto graphene paper by drop casting, build a high performance HER electrode exhibiting an overpotential of only 66 mV at current density of 10 mA cm^{-2} under alkaline conditions. Intrinsic activity of catalyst was evaluated by measuring the Tafel plot (as low as 82 mV/dec) and turnover frequencies (2.07 s^{-1} for a Pt loading of 11.2 μg cm^{-2}). The effect of Pt decoration has been modelled through energy band bending supported by electrochemical analyses. A full cell for alkaline electrochemical water splitting has been built, composed of Pt decorated NiO microflowers as cathode and bare NiO microflowers as anode, showing a low potential of 1.57 V to afford a current density of 10 mA cm^{-2} and a good long-term stability. The reported results pave the way towards an extensive utilization of Ni based nanostructures with ultralow Pt content for efficient electrochemical water splitting.

* *Corresponding author*.Dipartimento di Fisica e Astronomia "Ettore Majorana", Università degli Studi di Catania, via S. Sofia 64, 95123, Catania, Italy

E-mail address: salvo.mirabella@dfa.unict.it (S. Mirabella).

https://doi.org/10.1016/j.ijhydene.2022.08.005

Introduction

Electrochemical water splitting represents a promising strategy to provide sustainable clean energy source from the conversion of water into chemicals and fuels [1–5]. It is composed of two half reactions, hydrogen evolution reaction (HER) and oxygen evolution reaction (OER), both of which are potential candidates for future clean energy sources [1,3,6–9]. The main limiting factor of these reactions is represented by their sluggish kinetics [1,10,11].

The hydrogen evolution reaction (HER) is one of the most often studied electrocatalytic processes because of its industrial and technological interest for producing hydrogen gas through a limited number of reaction steps [12–14].

The reaction occurs at cathode via a two-electrons reaction [15]:

$$2H^+ + 2e^- \rightarrow H_2 \quad (1)$$

From an industrial perspective on water electrolysis, HER is often conducted in alkaline media to achieve higher stability of the catalyst materials [14]. In alkaline medium, HER proceeds through two steps [11,12,16,17]:

1. First, the catalyst splits a H_2O molecule (Volmer step) into a hydroxyl ion (OH^-) and an adsorbed hydrogen atom (H_{ads});
2. then, a hydrogen molecule is formed via either the interaction of the H_{ads} atom and water molecule (Heyrovsky step) or the combination of two H_{ads} atoms (Tafel step).

However, the kinetics of HER in alkaline medium are slow if compared with those in acid environment because of the low concentration of available protons. As a consequence, this process will require additional effort to obtain protons by water dissociation near or on electrode surface.

The state-of-art HER catalyst is platinum (Pt) and its alloys, but the scarcity and cost of Pt, universally considered a critical raw material, limit its large-scale application for electrolysis [15]. In past decades, extensive research has been focused on the development of practical alternatives to Pt, as efficient and renewable energy sources [16,18]. These have resulted in the identification of a variety of promising HER catalysts free of precious metals such as sulfides, phosphides, carbides, nitrides, selenides, and borides [3,19,20].

At the same time, enhancing the efficiency of noble metals utilization may also provide a realistic approach to the development of high-performance and cost-effective catalysts. While Pt is well-known to be effective for the adsorption of H_{ads} atoms, the overall sluggish HER kinetics in alkaline solutions stems from the insufficient catalyzing capability of Pt toward the cleavage of the H–OH bond. A possible solution consists in the creation of catalysts with a combination of metal oxides and Pt, where the oxides promote the dissociation of H_2O and the nearby Pt facilitates the adsorption and recombination of H_{ads} into molecular H_2 [15,18,21].

The transition metal oxide NiO is considered a valuable candidate as active material for electrochemical water splitting thanks to its Earth abundance and low cost [22]. Furthermore, NiO nanostructures (interconnected networks, nanosheets, microflowers) increase electrolyte permeability through the active material, making more favorable the mass transport at the electrode-solution interface [23]. Thanks to unique catalytic properties, nanostructured NiO is often used as a high-performance OER catalyst [24–27]. Recent literature reports also evidenced that NiO is particularly interesting due to its high stability for HER in alkaline electrolytes [4].

Heterostructured materials on the nanoscale have exhibited great potential in this area. These classes of catalysts, with double or multiple types of active sites on the surface, exhibit remarkable advantages for the HER in alkaline solutions. A synergistic electronic interaction between the metal and the oxide has been proposed as the reason for the enhanced HER performance [4,14,21]. In particular, Pt–NiO catalysts can be the key for designing efficient and cheap catalyst at which Pt favors H^+ adsorption and NiO promotes the adsorption of OH^- species [28,29].

Unfortunately, there are no reports on overall water splitting using only NiO-based materials (decorated or not) as bifunctional electrocatalysts, except for two ones [1,28]. Mondal et al. tested the performance of porous hollow nanostructured NiO electrodes for overall water splitting taking advantage of their high surface areas, porous microstructures, inner hollow architectures [1]. Similarly, Bian et al. synthesized a hierarchically structured Pt/NiO/Ni/CNTs with a low loading of Pt NPs for efficient OER and HER, taking advantage of the presence of the NiO/Ni heterojunction to boost the overall water splitting performance [28].

Here, we report a new strategy for overall water splitting electrodes, exploiting NiO nanostructures (microflowers, μFs) on graphene paper (GP), decorated with ultralow content of Pt nanoparticles (NPs). NiO μFs are synthesized by a chemical-based method and decorated with a colloidal solution of Pt NPs. Our hybrid metal-oxide catalyst unfolds outstanding activity toward HER, with an overpotential of 66 mV at a constant current density of 10 mA cm^{-2}. The present electrocatalyst shows a high rate of hydrogen generation as evidenced by the remarkable turnover frequency (TOF) values despite the low amount of loaded Pt. An alkaline electrolyzer is tested using Pt–NiO μFs electrode and undecorated NiO μFs as cathode and anode, respectively. We demonstrate that this all NiO-based electrolyzer can sustain a current density of 10 mA cm^{-2} with a potential of 1.57 V. The present work represents a valid strategy for the development of cost-effective electrocatalysts with a very small content of noble metal for widespread water electrocatalysis application.

Materials and methods

Synthesis of NiO microflowers and Pt nanoparticles

NiO microflowers (μFs) were synthesized from a chemical solution method trough a bain-marie configuration [24]. The obtained μFs powder were dispersed in an aqueous solution of deionized water and ethanol and sonicated for 15 min at room temperature to achieve a higher dispersion of the nanostructures.

Pt nanoparticles (NPs) dispersion was produced through a green chemical reduction method at room temperature with ascorbic acid (AA) as reducing agent [20]. 30 μL of 33 mM AA

were dispersed in 30 mL of 0.2 mM H_2PtCl_6 (Sigma-Aldrich, St. Louis, MO, USA, ≥99.9%) aqueous solution. The dispersion was then stirred for 5 min and used without further purification.

Preparation of the electrodes

Graphene paper (GP) substrates (1 × 1.5 cm^2, 240 nm thick, Sigma Aldrich, St. Louis, MO, USA) were rinsed with deionized water and ethanol and dried in N_2 to clean the surface from any impurity. NiO μFs were deposited by drop casting by using 20 μL of NiO dispersion. The samples were then dried on a hot plate at 80 °C for 10 min. Pt NPs were dispersed onto the electrode by subsequent addition of drops with NP dispersion in order to vary the catalyst loading. The mass of NiO (0.30 mg) on GP was measured by a Mettler Toledo MX5 Microbalance (sensitivity: 0.01 mg). Decorated samples are labelled according to the number of Pt dispersion drops (e.g. 5Pt–NiO indicates NiO catalyst decorated with 5 drops of Pt NPs dispersion).

Characterization of Pt decorated NiO microflowers

Surface morphology was analyzed by using a Scanning Electron Microscope (SEM, Gemini field emission SEM Carl Zeiss SUPRA 25, Carl Zeiss Microscopy GmbH, Jena, Germany). SEM images were analyzed by using ImageJ software [30].

Transmission electron microscopy (TEM) analyses of Pt decorated NiO μFs dispersed on a TEM grid were performed with a Cs-probe-corrected JEOL JEM ARM200F microscope at a primary beam energy of 200 keV operated in scanning TEM (STEM) mode and equipped with a 100 mm^2 silicon drift detector for energy dispersive X-ray (EDX) spectroscopy. For EDX elemental mapping, the Pt X-rays signal was collected by scanning the same region multiple times with a dwell time of 0.5 ms. TEM images and EDX spectra were analyzed by using DigitalMicrograph® software [31].

The evaluation of Pt amount on NiO μFs was analyzed by Rutherford backscattering spectrometry (RBS, 2.0 MeV He^+ beam at normal incidence) with a 165° backscattering angle by using a 3.5 MV HVEE Singletron accelerator system (High Voltage Engineering Europa, Netherlands). RBS spectra were analyzed by using XRump software [32].

Electrochemical measurements were carried out at room temperature by using a VersaSTAT 4 potentiostat (Princeton Applied Research, USA) and a three-electrode setup with a graphite rod as counter electrode, a saturated calomel electrode (SCE) as reference electrode, and the prepared electrodes as working electrodes. 1 M KOH (pH 14, Sigma Aldrich, St. Louis, MO, USA) was used as supporting electrolyte. Cyclic voltammetry (CV) curves were recorded at a scan rate of 10 mV s^{-1} in the potential range −0.7 ÷ −1.5 V vs SCE in order to stabilize the electrodes. The HER activities of decorated catalysts were investigated using linear sweep voltammetry (LSV) at scan rate of 5 mV s^{-1} in the same potential windows of CVs. Electrochemical impedance spectroscopy (EIS) was performed with a superimposed 10 mV sinusoidal voltage in the frequency range $10^4 \div 10^{-1}$ Hz at a potential just after the onset potential (E_{onset}, the minimum potential at which a reaction product is formed at an electrode). Tafel plots were extrapolated from polarization curves by plotting the overpotential (η) as a function of the log of the current density. Mott–Schottky (M–S) analyses were conducted on bare and decorated samples in the potential range 0–1 V vs. SCE, at 1000 Hz frequency. Chronopotentiometry (CP) analysis was employed to study the stability of the samples in a 1 M KOH solution for 15 h at a constant current density of 10 mA cm^{-2}.

Electrochemical data analysis

Current density was normalized to the geometrical surface area and measured potentials vs SCE were converted to the reversible hydrogen electrode (RHE) according to the equation [33]:

$$E_{RHE} = E_{SCE} + 0.059 \cdot pH + 0.244 \quad (2)$$

All measured potentials (η') were manually corrected by iR_u-compensation as follows:

$$\eta = \eta' - iR_u \quad (3)$$

where i is the electrode current and R_u [Ω] is the uncompensated resistance (extracted from EIS).

The turnover frequency (TOF) is defined as the rate of production of oxygen molecules per active site:

$$TOF = \frac{I}{2nF} \quad (4)$$

where I is the measured current at a fixed overpotential, the term 2 represents the number of electrons involved in the HER, F is the Faraday constant and n is the number of moles of the active sites [34]. Once the Pt amount is known, the number of active Pt moles can be calculated as follows:

$$n_{Pt}[\text{g cm}^{-2}] = \frac{\text{Dose}_{Pt}[\text{at cm}^{-2}]}{N_A[\text{at mol}^{-1}]} \quad (5)$$

where Dose_{Pt} is the RBS Dose, representing the amount of Pt atoms per cm^2, and N_A is the Avogadro's number.

Finally, the mass activity is defined by the ratio between a fixed current density and the catalyst loading (obtained by multiplying n_{Pt} for the atomic weight of the catalyst):

$$\text{Mass activity} = \frac{j[\text{A cm}^{-2}]}{\text{catalist loading [mg cm}^{-2}]} \quad (6)$$

Results and discussion

Morphological and elemental characterization

Fig. 1(a) shows SEM images of NiO μFs on GP. Our catalyst totally recovers the surface of graphene electrode with an irregular thickness due to the agglomeration of μFs. Fig. 1(b) of the same figure shows a tilted view of the electrode. After decoration, Pt NPs (mean size of 2 nm) spread onto NiO μFs (bright particles on STEM Z-contrast image in Fig. 1(c)). STEM EDX elemental map in Fig. 1(d) allowed us to confirm the effective presence of Pt decorating NiO catalyst. RBS analyses (Fig. 1(e)) confirmed Pt presence and allowed us to quantify the Pt loading, by using a flat substrate covered with the same drops containing Pt NP dispersion used for the electrode fabrication. We assume that after drop casting, the measured

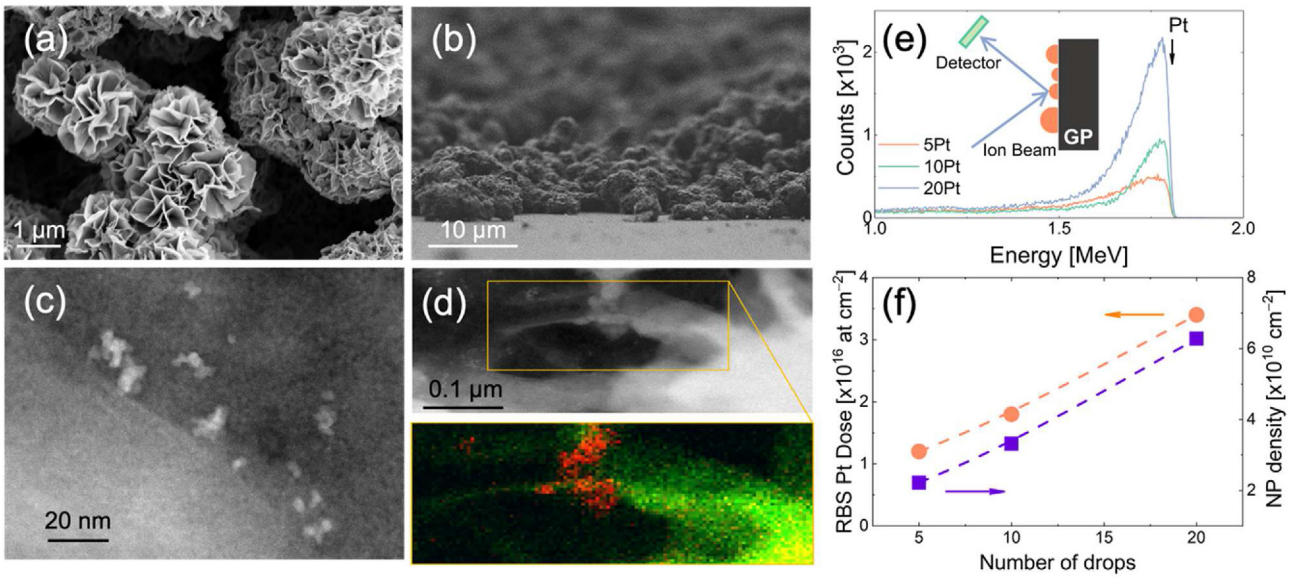

Fig. 1 – (a) SEM image of NiO μFs on GP; (b) tilted view of NiO Fs on GP; (c) STEM Z-contrast image of Pt NPs on NiO μFs (20Pt–NiO); (d) EDX elemental map of Pt NPs (red) on a single NiO sheet (green and yellow for Ni and O, respectively); (e) RBS spectra of Pt NPs on a flat GP substrate; (f) RBS Pt dose and NP density as a function of the number of Pt colloidal solution drops.

Table 1 – Amount of Pt NPs for different drops and HER parameters.

Sample	Pt RBS Dose [$\times 10^{16}$ at cm^{-2}]	Pt NP density [$\times 10^{8}$ NPs cm^{-2}]	Pt loading [μg cm^{-2}]	Overpotential [mV]	Tafel slope [mV dec^{-1}]
NiO	–	–	–	247	224
5Pt–NiO	1.20	1.0	3.9	206	260
10Pt–NiO	1.80	1.5	5.8	94	115
20Pt–NiO	3.40	2.9	11.2	66	82

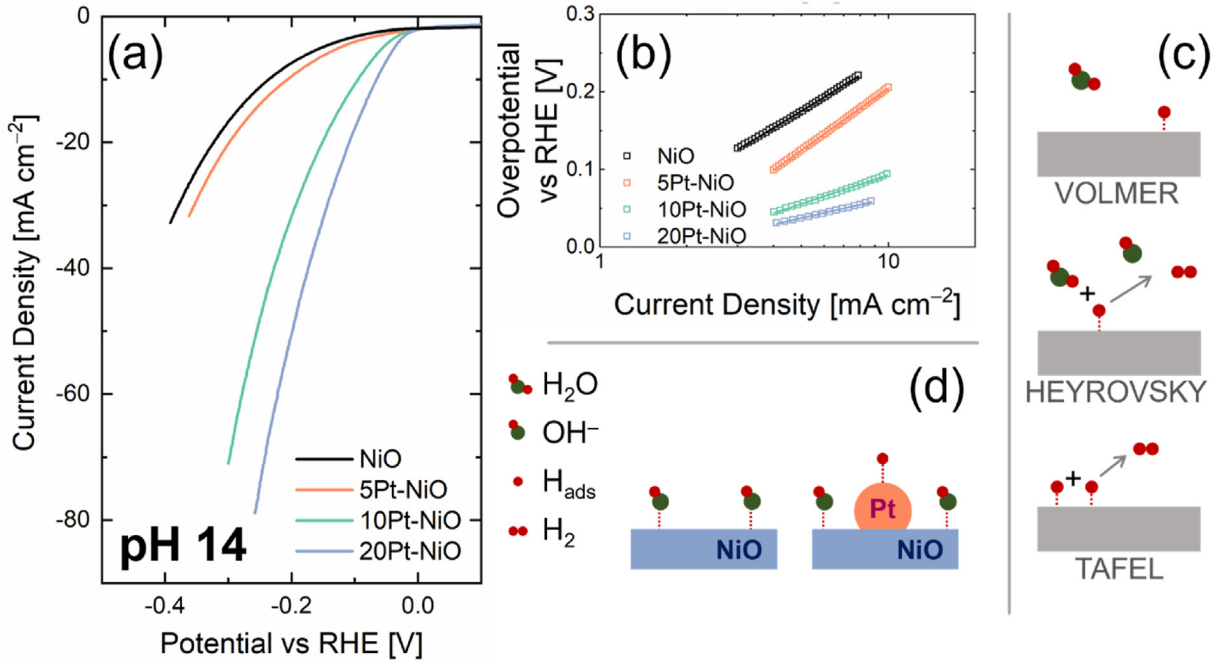

Fig. 2 – (a) Polarization curves, (b) Tafel plot of bare and decorated NiO μFs; (c) HER mechanisms; (d) HER mechanism at NiO and Pt–NiO electrodes.

Pt loading on a flat substrate is the same of that on NiO μFs. Moreover, this NP density is not dependent from the type of surface since it is an intrinsic quantity. The Pt loading is related to the area of Pt peak in the RBS spectrum (at around 1.8 MeV) [35]. As expected, Pt amount increases with the number of drops: 1.2×10^{16} at cm^{-2}, 1.8×10^{16} at cm^{-2}, 3.4×10^{16} at cm^{-2}, for 5, 10, and 20 drops, respectively (Fig. 1(f)). Pt NP density cannot be verified by SEM analysis because of the rough surface and shadowing effect caused by NiO nanostructures. Thus, the Pt amount (D_{RBS}, from RBS [34]) was joined with Pt NP diameter (Fig. S1) to evaluate the density N of NPs decorating NiO μFs, through the following relation [33,37]:

$$D_{RBS} = N\, \rho_{at}\, V_{NP} \quad (7)$$

where ρ_{at} is the Pt atomic bulk density (6.62×10^{22} at cm^{-3}) and V_{NP} is the volume of a single NP (in cm^3) based on the size of NPs (measured from SEM images). Following these considerations, the NP density was found to vary from 2×10^{10} NPs cm^{-2} to 6.2×10^{10} NPs cm^{-2} (Fig. 1(f)). Finally, from eq. (5) the Pt loading can be easily calculated, confirming the extremely low content of Pt in our decorated electrodes. The obtained values for RBS Pt dose, NP density, Pt loading are reported in Table 1.

Electrochemical characterization

To evaluate the electrochemical performance of bare and decorated NiO μFs on HER in alkaline conditions, electrochemical analyses were performed in 1 M KOH (Fig. 2). Polarization curves (Fig. 2(a)) clearly show how the presence of Pt drastically reduces the activation barrier for the H_2 production, confirmed by a variation in the onset potential and overpotential at a constant current density of 10 mA cm^{-2} from 247 to 66 mV (Table 1). Two types of behavior can be distinguished as a function of the quantity of Pt:

(i) for no (or ultralow) Pt loading, both overpotential and onset potential appear at relatively high voltages, indicating that high energies are required to overcome the adsorption of H^+ and subsequent production of H_2 steps;
(ii) by increasing the density of NPs (10Pt and 20Pt), overpotential and onset potential drastically reduce pointing out an enhanced catalytic action of Pt against HER.

The morphology of samples after HER was compared to the pristine ones, as shown in Fig. S1, without any significant morphology variation.

Tafel slopes of Pt decorated NiO μFs are reported in Fig. 2(c). Pt decoration leads to a decrease of Tafel slope to a value of 82 mV dec^{-1} for 20Pt–NiO sample. Tafel slope values allow a deep understanding of HER catalytic mechanism. Three possible pathways (illustrated in Fig. 2(d)) for the HER reaction in alkaline medium can be distinguished [11,12,38]:

(i) electrochemical hydrogen adsorption (Volmer step, $H_2O + e^- \rightarrow H_{ads} + OH^-$) at the active site of the catalyst;
(ii) H_2 formation through an electrochemical desorption step (Heyrovsky step, $H_{ads} + H_2O + e^- \rightarrow H_2 + OH^-$);
(iii) H_2 formation through a recombination step between two adsorbed hydrogen atoms (Tafel step: $H_{ads} + H_{ads} \rightarrow H_2$).

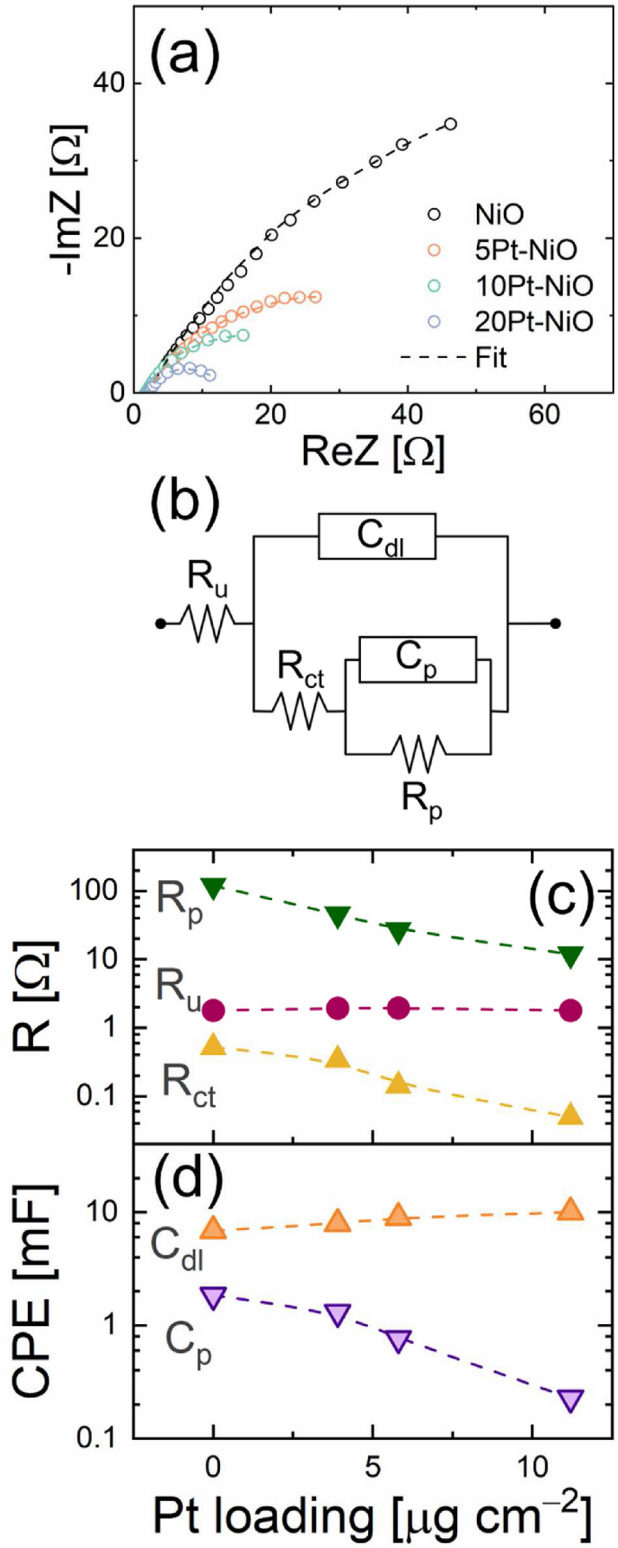

Fig. 3 – (a) Nyquist plot for bare and decorated electrodes; (b) Armstrong and Henderson equivalent circuit used to fit the experimental data; (c, d) behavior of equivalent circuit elements as a function of mass loading.

Usually, the rate-determining step (RDS) can be evaluated from the value of the Tafel slope [35–37,39–41]. Our values (by considering the kinetic analysis and mechanism for HER that are based on Butler-Volmer equation [39]) suggest that the RDS for our catalysts is represented by Volmer step and by the initial hydrogen adsorption. NiO-based materials have been widely proved to be optimal catalysts for OH^- adsorption [21,28,29]. The high Tafel slope value for bare semiconductor electrode clearly demonstrates that the HER proceeds much slower in NiO sample Conversely, Pt loading causes a reduction of Tafel slopes (Fig. 2(e)). This evidence suggests that HER is limited by the hydrogen adsorption, with a poor efficiency in the NiO case. Conversely, the presence of Pt in decorated catalysts reveals an enhanced adsorption of hydrogen atoms on the surface. Pt decoration not only reduces the activation barrier for the activation of the HER (evidenced by the lowest overpotential for the most decorated sample), but also favors the hydrogen adsorption at the catalyst surface.

Nyquist plots from EIS analysis in Fig. 3(a) remark the role of Pt NPs in the HER. They were acquired in the so-called turnover region, just after the onset potential of each sample in order to appreciate a good HER activity [24,42]. The experimental EIS spectra were fitted (continuous lines) by the Armstrong-Henderson equivalent circuit [43] (Fig. 3(b)) and the extracted fitting parameters are reported in Fig. 3(c and d). In the Armstrong-Henderson circuit different elements can be recognized [13,16,17,24,42,44–48]:

1. R_u is the uncompensated resistance;
2. R_{ct} is the charge transfer resistance at the electrode-electrolyte interface;
3. C_{dl} is the double layer capacitance (here we used constant phase elements to take into account the non-ideal behavior of the nanostructured electrodes);
4. R_p is strictly related with the mass transfer resistance of adsorbed intermediate H_{ads} (in particular it well describes the adsorption/desorption of intermediates at the electrode surfaces);
5. C_p is the H_{ads} related capacitance (usually called pseudo-capacitance) in the HER mechanism.

The adequately fitted experimental data reveal how these 5 parameters vary with Pt decoration (Fig. 3(c and d)). R_u and C_{dl} do not appreciably change, as expected since the Pt NPs coverage is quite limited and most of the interface among NiO μFs and electrolyte is unchanged. A clear reduction in both R_{ct} and R_p with Pt loading indicates that Pt accelerates the electron transfer kinetics, probably enhancing the availability of electrons at surface. C_p, related to H_{ads} adsorption, decreases as the amount of Pt increases. Pt NPs act as effective active sites for hydrogen adsorption. Consequently, the higher the number of active sites, the lower their occupancy and therefore the value of C_p.

To quantitatively evaluate the effect of Pt decoration of NiO μFs we performed Mott–Schottky (M–S) analysis (SI for

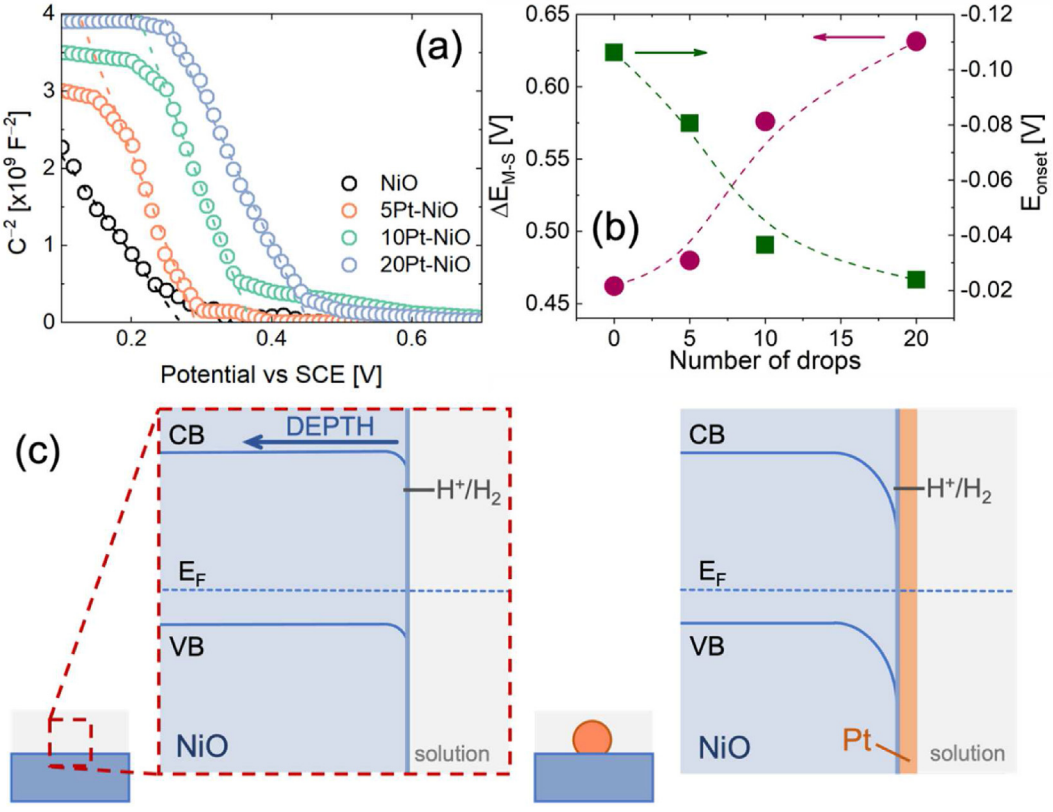

Fig. 4 – (a) Mott-Schottky plot of bare and Pt-decorated NiO electrodes; (b) variation of NiO energy band bending and onset potential as a function of the number of Pt solution drops; (c) scheme of the modification of energy levels at the semiconductor-electrolyte interface for bare NiO and Pt–NiO catalysts.

details). The M–S plot typically reports the inverse of squared capacitance (C^{-2}) measured as a function of potential applied to the sample, as reported in Fig. 4(a) [24,49–54]. By increasing E, C^{-2} goes to zero as the applied potential increases, indicating the presence of a capacitance at the electrode-electrolyte interface. Such behavior is typical of a *p*-type semiconductor, as NiO is [55,56]. The intercept with *x*-axis (E_{FB}) represents the so-called flat band potential [49–54,57–59]. For a planar semiconductor electrode, the quantity $\Delta E_{M-S} = E_{FB} - E_{OC}$ (where E_{OC} is the open circuit potential) represents the bending of the semiconductor energy bands [24] resulting from the alignment of the Fermi level of the electrode and the redox potential of the electrolyte (violet points in Fig. 4(b)). After the loading of Pt NPs, we observed a clear shift of E_{FB} towards more positive potential, up to 0.454 V in 20Pt–NiO case (Table 2). Even if our electrodes are nanostructured semiconductors, such evidence reveals a considerable difference in energy band bending due to Pt decoration. Moreover, it is possible to correlate the effect of decoration on energy band position of NiO with catalytic properties of the electrodes by considering the value of onset potential (E_{onset}, green points in Fig. 4(b)). Onset potential is usually considered an important indicator for the catalytic activity along with the exchange current density in electrocatalysis [34]. For a cathodic reaction, onset potential is the highest potential at which a reaction product (H_2 in our case) is formed at an electrode [60]. A commonly used method for the determination of this value is the intersection point between the tangent lines of the Faradaic and non-Faradaic [60–62]. Fig. 4(b) clarifies the effect of Pt loading on ΔE_{M-S} and E_{onset}. As the amount of Pt NPs increases, the energy band bending grows, index of the creation of a nano Schottky junction at the metal-semiconductor interface [24]. Pt decoration increases the energy band bending, because of electron spillover effects, leading to space charge regions and localized electric field [37]. At the same time, a drastic reduction of E_{onset} is observed in presence of Pt NPs. These two evidences confirm that surface decoration of NiO μFs is highly effective in tuning the catalytic properties of our nanostructured electrode. The increase in bending of semiconductor energy levels leads to accumulation of electrons below the semiconductor surface, considerably reducing the activation barrier for H_2 production (as described in eq. (1) and demonstrated by the decreased values of E_{onset} for 10Pt and 20Pt–NiO electrodes) and making the HER mechanism more favorable at lower overpotentials.

Fig. 4(c) schematizes the effect of Pt loading on NiO band position at the electrode-electrolyte interface.

TOF is a crucial parameter for evaluating the HER performance of a catalyst because it reflects the intrinsic electrocatalytic activity of the electrode [2,20,34,63]. As presented in Fig. 5(a), Pt-decorated samples show markedly high TOF values. It is worth to note that the TOF value of 2.07 s^{-1} (at an overpotential of 50 mV) found for 20Pt–NiO is comparable (and even superior) to those reported in literature and confirms that the present Pt NP decorated catalyst owns extraordinary efficiency of hydrogen generation (see Table S1).

The obtained results are now compared with the state-of-art. Fig. 5(b) shows the comparison of mass activity measured at 10 mA cm^{-2} and the overpotential for 10 mA cm^{-2} (based on geometric area) for our decorated electrodes with other Pt-based catalysts under alkaline conditions [2]. In our samples, an increase of the mass loading leads to a reduction of the overpotential for the HER, without a significant decrease of intrinsic activity. This comparison, together with the TOF values, makes our Pt decorated NiO μFs valuable candidates as cathode electrodes for the HER.

Table 2 – Values of open circuit potential, flat band potential, energy barrier, and onset potential for bare and decorated samples.

Sample	Pt drops	E_{OC} [V]	E_{FB} [V]	ΔE_{M-S} [V]	E_{onset} [V]
NiO	–	−0.192	0.270	0.462	−0.106
5Pt–NiO	5	−0.187	0.292	0.479	−0.081
10Pt–NiO	10	−0.206	0.370	0.576	−0.036
20Pt–NiO	20	−0.178	0.454	0.632	−0.024

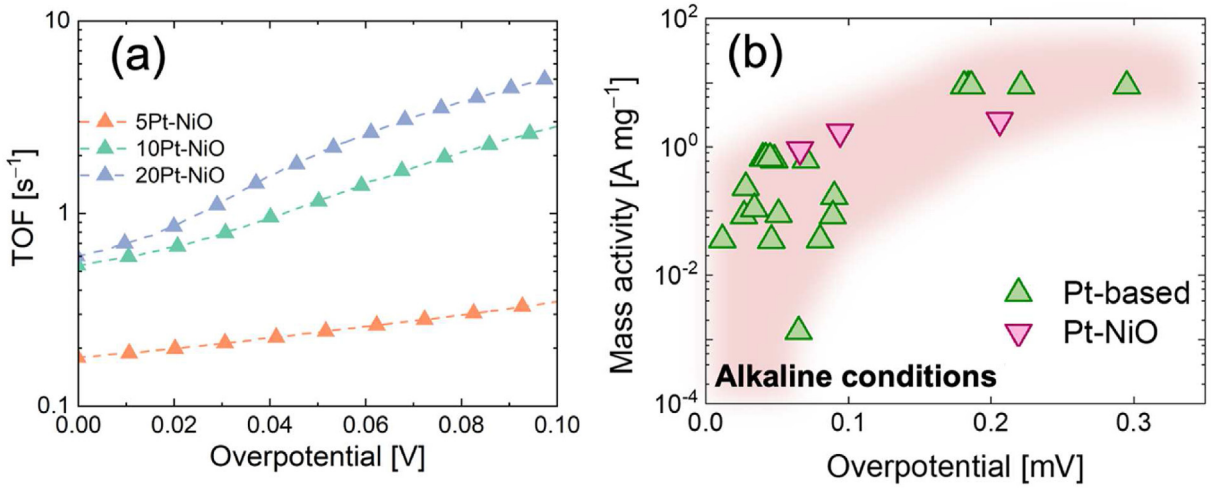

Fig. 5 – (a) TOF of Pt–NiO catalysts on GP; mass activity at 10 mA cm^{-2} as a function of the overpotential and the catalyst loading [adapted from 2].

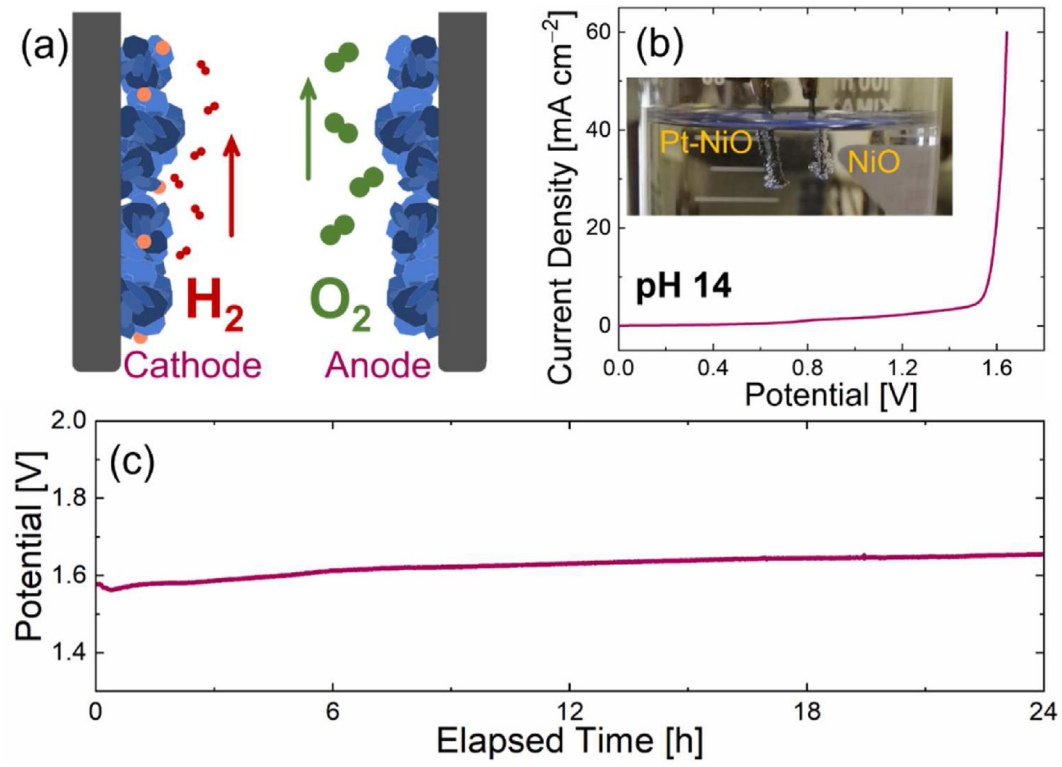

Fig. 6 – (a) Polarization curve of the two-electrode electrolyzer Pt–NiO||NiO for overall water splitting under alkaline condition (1 M KOH, pH 14); (b) long-term chronopotentiometric stability test of Pt–NiO||NiO.

Table 3 – Summary of various Ni-based Electrocatalysts for Overall Water Splitting.

Catalyst material	Electrolyte	Overall water splitting overpotential at 10 mA cm^{-2} [V]	Ref.
Pt/NiO/Ni/CNT-3||Pt/NiO/Ni/CNT-3	1 M KOH	1.61	[64]
NiO/Ni-CNT||NiFe LDH	1 M KOH	1.50 (20 mA cm^{-2})	[65]
Pt/Ni–P/NF||Ni–P/NF	1 M KOH	1.64	[20]
Pt–NiO||NiO	1 M KOH	1.57	This work

Motivated by the excellent HER performance of catalysts and the high OER activity of our previously reported NiO μFs on GP [24], we investigated the overall water-splitting performance under alkaline condition by employing 20Pt–NiO μFs as the cathode and NiO μFs as the anode (a scheme of the Pt–NiO||NiO is reported in Fig. 6(a)). Our as-constructed alkaline electrolytic cell requires a low potential of 1.57 V to afford a current density of 10 mA cm^{-2} (Fig. 6(b)) and Supplementary Video 1, which is comparable or smaller to other electrocatalysts reported in Table 3.

Supplementary video related to this article can be found at https://doi.org/10.1016/j.ijhydene.2022.08.005.

In addition, the overall water-splitting durability of the two electrodes was tested using chronopotentiometry for 24 h (Fig. 6(c)) showing a good stability over prolonged times (with an increase of overpotential of 50 mV after 24 h).

Our results reveal that the present Pt–NO||NiO electrodes represent highly efficient electrocatalysts.

Conclusions

In conclusion, we developed a high-efficiency HER catalyst by synthesizing low-content Pt-NP decorated low-cost NiO microflowers (μFs) onto a graphene paper substrate. By varying the loading of Pt NPs, the role of decoration on catalytic performance of the materials was elucidated in terms of energy band bending of NiO and density of active sites. The Pt–NiO catalyst with optimized NP loading shows an overpotential of only 66 mV at current density of 10 mA cm^{-2} and a promisingly low Tafel slope of 82 mV dec^{-1}. The performance of NiO μFs were also supported by high intrinsic activity, in terms of TOF of 2.07 s^{-1} at an overpotential of 50 mV. An alkaline all NiO-based electrolyzer was developed by using Pt–NiO as cathode and bare NiO as anode, requiring a low potential of 1.57 V to afford a current density of 10 mA cm^{-2} and a good long-term stability. The high activity, and low-cost of the present Pt–NiO μFs pave the way for large-scale and long-term applications of NiO-based catalysts for overall water splitting.

Author contributions

L.B. fabricated the nanostructured electrode, acquired and analyzed data, generated the figures, and drafted the manuscript; S.B. analyzed the electrochemical data; M.S. performed STEM and EDX analysis; A.T., F.P., and S.M.: conceived the idea, contributed to data analysis and interpretation; S.M. supervised the project. All authors have given approval to the final version of the manuscript.

Fundings

This research was funded by the project AIM1804097–Programma Operativo Nazionale FSE –FESR "Ricerca e Innovazione 2014–2020" and was supported by the project "Programma di ricerca di ateneo UNICT 2020-22" linea 2.

Declaration of competing interest

The authors declare that they have no known competing financial interests or personal relationships that could have appeared to influence the work reported in this paper.

Acknowledgments

The authors wish to thank G. Pantè and S. Tatì (CNR-IMM Catania, Italy) for technical support.

Appendix A. Supplementary data

Supplementary data to this article can be found online at https://doi.org/10.1016/j.ijhydene.2022.08.005.

REFERENCES

[1] Mondal A, Paul A, Srivastava DN, Panda AB. NiO hollow microspheres as efficient bifunctional electrocatalysts for Overall Water-Splitting. Int J Hydrogen Energy 2018. https://doi.org/10.1016/j.ijhydene.2018.06.139.
[2] Kibsgaard J, Chorkendorff I. Considerations for the scaling-up of water splitting catalysts. Nat Energy 2019. https://doi.org/10.1038/s41560-019-0407-1.
[3] Bu X, Wei R, Gao W, Lan C, Ho JC. A unique sandwich structure of a CoMnP/Ni2P/NiFe electrocatalyst for highly efficient overall water splitting. J Mater Chem 2019. https://doi.org/10.1039/c9ta02551k.
[4] Faid AY, Barnett AO, Seland F, Sunde S. Ni/NiO nanosheets for alkaline hydrogen evolution reaction: in situ electrochemical-Raman study. Electrochim Acta 2020. https://doi.org/10.1016/j.electacta.2020.137040.
[5] Li X, Zhao L, Yu J, Liu X, Zhang X, Liu H, et al. Water splitting: from electrode to green energy system. Nano-Micro Lett 2020. https://doi.org/10.1007/s40820-020-00469-3.
[6] Doyle RL, Lyons MEG. The oxygen evolution reaction: mechanistic concepts and catalyst design. Photoelectrochem Sol Fuel Prod 2016. https://doi.org/10.1007/978-3-319-29641-8_2.
[7] Liu FQ, Liu JW, Gao Z, Wang L, Fu XZ, Yang LX, et al. Constructing bimetal-complex based hydrogen-bonded framework for highly efficient electrocatalytic water splitting. Appl Catal B Environ 2019. https://doi.org/10.1016/j.apcatb.2019.117973.
[8] Gao Z, Xiao L, Su X, He X, Yu Y, Huang X, et al. Carambola-like metal-organic frameworks for high-performance electrocatalytic oxygen evolution reaction. J Energy Chem 2020. https://doi.org/10.1016/j.jechem.2020.05.023.
[9] Gao Z, Yu Z, Huang Y, He X, Su X, Xiao L, et al. Flexible and robust bimetallic covalent organic frameworks for the reversible switching of electrocatalytic oxygen evolution activity. J Mater Chem 2020. https://doi.org/10.1039/c9ta14023a.
[10] Suen NT, Hung SF, Quan Q, Zhang N, Xu YJ, Chen HM. Electrocatalysis for the oxygen evolution reaction: recent development and future perspectives. Chem Soc Rev 2017. https://doi.org/10.1039/c6cs00328a.
[11] Safizadeh F, Ghali E, Houlachi G. Electrocatalysis developments for hydrogen evolution reaction in alkaline solutions – a review. Int J Hydrogen Energy 2015. https://doi.org/10.1016/j.ijhydene.2014.10.109.
[12] Lasia A. Mechanism and kinetics of the hydrogen evolution reaction. Int J Hydrogen Energy 2019. https://doi.org/10.1016/j.ijhydene.2019.05.183.
[13] Franceschini EA, Lacconi GI, Corti HR. Kinetics of the hydrogen evolution on nickel in alkaline solution: new insight from rotating disk electrode and impedance spectroscopy analysis. Electrochim Acta 2015. https://doi.org/10.1016/j.electacta.2015.01.110.
[14] Wei J, Zhou M, Long A, Xue Y, Liao H, Wei C, et al. Heterostructured electrocatalysts for hydrogen evolution reaction under alkaline conditions. Nano-Micro Lett 2018. https://doi.org/10.1007/s40820-018-0229-x.
[15] Stephens IEL, Chorkendorff I. Minimizing the use of platinum in hydrogen-evolving electrodes. Angew Chem Int Ed 2011. https://doi.org/10.1002/anie.201005921.
[16] Doyle RL, Godwin IJ, Brandon MP, Lyons MEG. Redox and electrochemical water splitting catalytic properties of hydrated metal oxide modified electrodes. Phys Chem Chem Phys 2013. https://doi.org/10.1039/c3cp51213d.
[17] Nikolic VM, Maslovara SL, Tasic GS, Brdaric TP, Lausevic PZ, Radak BB, et al. Kinetics of hydrogen evolution reaction in alkaline electrolysis on a Ni cathode in the presence of Ni-Co-Mo based ionic activators. Appl Catal B Environ 2015. https://doi.org/10.1016/j.apcatb.2015.05.012.
[18] Chen ZJ, Cao GX, Gan LY, Dai H, Xu N, Zang MJ, et al. Highly dispersed platinum on honeycomb-like NiO@Ni film as a synergistic electrocatalyst for the hydrogen evolution reaction. ACS Catal 2018. https://doi.org/10.1021/acscatal.8b02212.
[19] Hou Y, Lohe MR, Zhang J, Liu S, Zhuang X, Feng X. Vertically oriented cobalt selenide/NiFe layered-double-hydroxide nanosheets supported on exfoliated graphene foil: an efficient 3D electrode for overall water splitting. Energy Environ Sci 2016. https://doi.org/10.1039/c5ee03440j.
[20] Battiato S, Bruno L, Terrasi A, Mirabella S. Superior performances of electroless-deposited Ni-P films decorated with an ultralow content of Pt for water-splitting reactions. ACS Appl Energy Mater 2022. https://doi.org/10.1021/acsaem.1c03880.
[21] Subbaraman R, Tripkovic D, Chang KC, Strmcnik D, Paulikas AP, Hirunsit P, et al. Trends in activity for the water electrolyser reactions on 3d M(Ni,Co,Fe,Mn) hydr(oxy)oxide catalysts. Nat Mater 2012. https://doi.org/10.1038/nmat3313.

[22] Gong M, Wang DY, Chen CC, Hwang BJ, Dai H. A mini review on nickel-based electrocatalysts for alkaline hydrogen evolution reaction. Nano Res 2016. https://doi.org/10.1007/s12274-015-0965-x.
[23] Silva VD, Simões TA, Grilo JPF, Medeiros ES, Macedo DA. Impact of the NiO nanostructure morphology on the oxygen evolution reaction catalysis. J Mater Sci 2020. https://doi.org/10.1007/s10853-020-04481-1.
[24] Bruno L, Scuderi M, Priolo F, Mirabella S. Enhanced electrocatalytic activity of low-cost NiO microflowers on graphene paper for oxygen evolution reaction. Sustain Energy Fuels 2022. https://doi.org/10.1039/D2SE00829G. In press.
[25] Cosentino S, Urso M, Torrisi G, Battiato S, Priolo F, Terrasi A, et al. High intrinsic activity of the oxygen evolution reaction in low-cost NiO nanowall electrocatalysts. Mater Adv 2020. https://doi.org/10.1039/d0ma00467g.
[26] Manivasakan P, Ramasamy P, Kim J. Reactive-template fabrication of porous NiO nanowires for electrocatalytic O2 evolution reaction. RSC Adv 2015. https://doi.org/10.1039/c5ra01739d.
[27] Yuan W, Li C, Zhao M, Zhang J, Li CM, Jiang SP. In situ self-assembled 3-D interconnected pristine graphene supported NiO nanosheets as superior catalysts for oxygen evolution. Electrochim Acta 2020. https://doi.org/10.1016/j.electacta.2020.136118.
[28] Bian Y, Wang H, Gao Z, Hu J, Liu D, Dai L. A facile approach to high-performance trifunctional electrocatalysts by substrate-enhanced electroless deposition of Pt/NiO/Ni on carbon nanotubes. Nanoscale 2020. https://doi.org/10.1039/d0nr03378b.
[29] Li Q, Cheng W, Zeng C, Zheng X, Sun L, Jiang Q, et al. Facile and rapid synthesis of Pt-NiOx/NiF composites as a highly efficient electrocatalyst for alkaline hydrogen evolution. Int J Hydrogen Energy 2022. https://doi.org/10.1016/j.ijhydene.2021.12.101.
[30] ImageJ. Available on https://imagej.nih.gov/ij/index.html.
[31] DigitalMicrograph®. Available online: https://www.gatan.com/products/tem-analysis/gatan-microscopy-suite-software.
[32] Thompson, M. Xrump. Available online: www.genplot.com.
[33] Stevens MB, Enman LJ, Batchellor AS, Cosby MR, Vise AE, Trang CDM, et al. Measurement techniques for the study of thin film heterogeneous water oxidation electrocatalysts. Chem Mater 2017. https://doi.org/10.1021/acs.chemmater.6b02796.
[34] Anantharaj S, Karthik PE, Noda S. The significance of properly reporting turnover frequency in electrocatalysis research. Angew Chem Int Ed 2021. https://doi.org/10.1002/anie.202110352.
[35] Alford TL, Feldman LC, Mayer JW. Fundamentals of nanoscale film analysis. 2007. https://doi.org/10.1007/978-0-387-29261-8.
[36] Bruno L, Urso M, Shacham-Diamand Y, Priolo F, Mirabella S. Role of substrate in au nanoparticle decoration by electroless deposition. Nanomaterials 2020;10. https://doi.org/10.3390/nano10112180.
[37] Bruno L, Strano V, Scuderi M, Franzò G, Priolo F, Mirabella S. Localized energy band bending in ZnO nanorods decorated with Au nanoparticles. Nanomaterials 2021;11:2718. https://doi.org/10.3390/nano11102718.
[38] Zheng Y, Jiao Y, Vasileff A, Qiao SZ. The hydrogen evolution reaction in alkaline solution: from theory, single crystal models, to practical electrocatalysts. Angew Chem Int Ed 2018. https://doi.org/10.1002/anie.201710556.
[39] Tian X, Zhao P, Sheng W. Hydrogen evolution and oxidation: mechanistic studies and material advances. Adv Mater 2019. https://doi.org/10.1002/adma.201808066.
[40] Shinagawa T, Garcia-Esparza AT, Takanabe K. Insight on Tafel slopes from a microkinetic analysis of aqueous electrocatalysis for energy conversion. Sci Rep 2015. https://doi.org/10.1038/srep13801.
[41] Murthy AP, Theerthagiri J, Madhavan J. Insights on Tafel constant in the analysis of hydrogen evolution reaction. J Phys Chem C 2018. https://doi.org/10.1021/acs.jpcc.8b07763.
[42] Anantharaj S, Noda S. Appropriate use of electrochemical impedance spectroscopy in water splitting electrocatalysis. Chemelectrochem 2020. https://doi.org/10.1002/celc.202000515.
[43] Armstrong RD, Henderson M. Impedance plane display of a reaction with an adsorbed intermediate. J Electroanal Chem 1972. https://doi.org/10.1016/S0022-0728(72)80477-7.
[44] Castro EB, Gervasi CA, Vilche JR. Oxygen evolution on electrodeposited cobalt oxides. J Appl Electrochem 1998. https://doi.org/10.1023/A:1003488409147.
[45] Conway BE, Liu TC. Characterization of electrocatalysis in the oxygen evolution reaction at platinum by evaluation of behavior of surface intermediate states at the oxide film. Langmuir 1990. https://doi.org/10.1021/la00091a044.
[46] Krstajić N, Popović M, Grgur B, Vojnović M, Šepa D. On the kinetics of the hydrogen evolution reaction on nickel in alkaline solution – part I. The mechanism. J Electroanal Chem 2001. https://doi.org/10.1016/S0022-0728(01)00590-3.
[47] Lyons MEG, Brandon MP. Int J Electrochem Sci 2008;3:1425–62.
[48] Wu G, Li N, Zhou DR, Mitsuo K, Xu BQ. Anodically electrodeposited Co+Ni mixed oxide electrode: preparation and electrocatalytic activity for oxygen evolution in alkaline media. J Solid State Chem 2004. https://doi.org/10.1016/j.jssc.2004.06.027.
[49] Bott AW. Electrochemistry of semiconductors. Curr Sep 1998;17:3.
[50] Beranek R. (Photo)electrochemical methods for the determination of the band edge positions of TiO 2-based nanomaterials. Adv Phys Chem 2011. https://doi.org/10.1155/2011/786759.
[51] Fabregat-Santiago F, Garcia-Belmonte G, Bisquert J, Bogdanoff P, Zaban A. Mott-Schottky analysis of nanoporous semiconductor electrodes in dielectric state deposited on SnO[sub 2](F) conducting substrates. J Electrochem Soc 2003. https://doi.org/10.1149/1.1568741.
[52] Hankin A, Bedoya-Lora FE, Alexander JC, Regoutz A, Kelsall GH. Flat band potential determination: avoiding the pitfalls. J Mater Chem 2019. https://doi.org/10.1039/c9ta09569a.
[53] Memming R. Semiconductor electrochemistry. 2000. https://doi.org/10.1002/9783527613069.
[54] Scholz F. Electroanalytical methods: guide to experiments and applications. 2010. https://doi.org/10.1007/978-3-642-02915-8.
[55] Hall DS, Lockwood DJ, Bock C, MacDougall BR. Nickel hydroxides and related materials: a review of their structures, synthesis and properties. Proc R Soc A Math Phys Eng Sci 2015. https://doi.org/10.1098/rspa.2014.0792.
[56] Ash B, Nalajala VS, Popuri AK, Subbaiah T, Minakshi M. Perspectives on nickel hydroxide electrodes suitable for rechargeable batteries: electrolytic vs. chemical synthesis routes. Nanomaterials 2020. https://doi.org/10.3390/nano10091878.
[57] Xu P, Milstein TJ, Mallouk TE. Flat-band potentials of molecularly thin metal oxide nanosheets. ACS Appl Mater Interfaces 2016. https://doi.org/10.1021/acsami.6b02901.
[58] Gelderman K, Lee L, Donne SW. Flat-band potential of a semiconductor: using the Mott-Schottky equation. J Chem Educ 2007. https://doi.org/10.1021/ed084p685.

[59] Darowicki K, Krakowiak S, Ślepski P. Selection of measurement frequency in Mott-Schottky analysis of passive layer on nickel. Electrochim Acta 2006. https://doi.org/10.1016/j.electacta.2005.04.079.
[60] Florent M, Wallace R, Bandosz TJ. Oxygen electroreduction on nanoporous carbons: textural features vs nitrogen and boron catalytic centers. ChemCatChem 2019. https://doi.org/10.1002/cctc.201801675.
[61] Blasco-Ahicart M, Soriano-Lopez J, Carbo JJ, Poblet JM, Galan-Mascaros JR. Polyoxometalate electrocatalysts based on earthabundant metals for efficient water oxidation in acidic media. Nat Chem 2018. https://doi.org/10.1038/NCHEM.2874.
[62] Lu G, Yang H, Zhu Y, Huggins T, Ren ZJ, Liu Z, et al. Synthesis of a conjugated porous Co(ii) porphyrinylene-ethynylene framework through alkyne metathesis and its catalytic activity study. J Mater Chem 2015. https://doi.org/10.1039/c4ta06231k.
[63] Battiato S, Urso M, Cosentino S, Pellegrino AL, Mirabella S, Terrasi A. Optimization of oxygen evolution reaction with electroless deposited Ni–P catalytic nanocoating. Nanomaterials 2021. https://doi.org/10.3390/nano11113010.
[64] Bian Y, Wang H, Gao Z, Hu J, Liu D, Dai L. A facile approach to high-performance trifunctional electrocatalysts by substrate-enhanced electroless deposition of Pt/NiO/Ni on carbon nanotubes. Nanoscale 2020. https://doi.org/10.1039/d0nr03378b.
[65] Gong M, Zhou W, Tsai MC, Zhou J, Guan M, Lin MC, et al. Nanoscale nickel oxide/nickel heterostructures for active hydrogen evolution electrocatalysis. Nat Commun 2014. https://doi.org/10.1038/ncomms5695.